Observations and Measurements on Unsteady Cloud Cavitation Flow Structures

L X Gu[1], G J Yan[1], B Huang[2]
[1] Beijing Institute of Astronautical System Engineering, Beijing, 100076, China
[2] Beijing Institute of Technology, Beijing 100081, China

E-mail: huangbiao@bit.edu.cn

Abstact The objectives of this paper are to investigate the unsteady structures and hydrodynamics of cavitating flows. Experimental results are presented for a Clark-Y hydrofoil, which is fixed at α=0°, 5° and 8°. The high-speed video camera and Particle Image Velocimetry (PIV) are applied to investigate the transient flow structures. The dynamic measurement system is used to record the dynamic characteristics. The cloud cavitation exhibits noticeable unsteady characteristics. For the case of α=0°, there exit strong interactions between the attached cavity and the re-entrant flow. While for the case of α=8°, the re-entrant flow is relatively thin and the interaction between the cavity and re-entrant flow is limited. The results also present that the periodic collapse and shedding of the large-scale cloud cavitation, which leads to substantial increase of turbulent velocity fluctuations in the cavity region. Experimental evidence indicates that the hydrodynamics are clearly affected by the cavitating flow structures, the amplitude of load fluctuation are much higher for the cloud cavitating cases.

1. Introduction

It is well known that unsteady cavitating flow in turbomachineries and controlled surface would lead to many problems such as sudden changes in loads, pressure pulsation, vibrations and noise [1-2]. Among the various cavitation phenomenons, more attention has been paid to the cloud cavitation due to the unsteady characteristics [3-4]. Various experimental studies have been conducted to improve the understanding of the complex structures and unsteady hydrodynamics of cloud cavitating flows. Li et al. [5] employed a PIV method to examine the structures of developed cavitating flows. They showed that strong mass and momentum transfers occurs between the upper and lower flow layers, which leads to the lower velocity distribution in the core part of the cavitating region. Shridhar and Katz [6] used fluorescent tracer particles and an optical filter to cancel the incident laser light and measured the velocity filed in the wake of a cloud cavity. Reynolds shear stresses were found been increased by 25 to 40% due to cavitation.

Although much works have explored the effects of cavitation through experimental studies, the complex flow structure and hydrodynamic characteristics of unsteady cloud cavitation are still not well understood. The objective of the present study is to obtain a comprehensive set of flow field data, video recordings and load coefficients to investigate the structures and hydrodynamics of unsteady cloud cavitation with various angles of attack.

[2] To whom any correspondence should be addressed.

2. Experimental set-up

Experimental studies are conducted in a closed-loop cavitation tunnel at Beijing Institute of Technology [7]. The schematic of experimental setup is illustrated in figure 1. The cavitation phenomenon is documented by a high-speed digital camera (HG-LE, by Redlake), with 4000 fps used in this study. A two-component high-speed PIV system provided by Dantec is used. The recording rate of 2000 Hz (4000 fps) at 1024×512 pixel is used for the actual data acquisition. The lift and drag are measured by four strain gauges of a dynamic measurement device [7], as shown in figure 2. Signals are amplified, filtered and collected through an 8-channel 16-bit A/D digitizer at simultaneous sample with a maximum available sample frequency of 51.2 kHz. A Clark-Y hydrofoil with different angles of attack is adopted in the present study, and the chord length of the hydrofoil is c=0.07 m. The position of the hydrofoil inside the test section is shown in figure 3. In this experimental research, the reference velocity U_∞ is fixed at 10m/s and the Reynolds number is $Re = U_\infty c/\nu = 7\times10^5$.

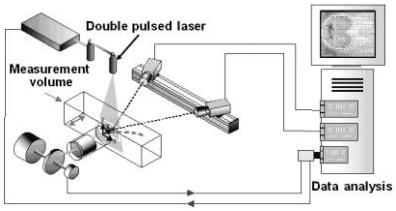

Figure 1 Schematic of the cavitation tunnel

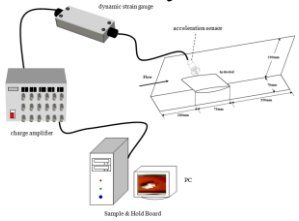

Figure 2 The schematic diagram of the dynamic measurement system

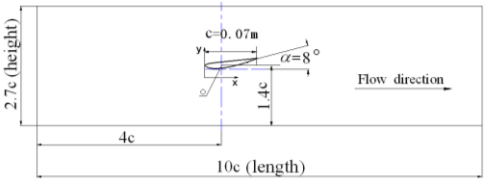

Figure 3 Sketch of the test section

3. Results and discussion

3.1. The unsteady multiphase structures with cloud cavitating flows

Figure 4 shows the side views of the periodic cavity structures, within a single flow cycle for all the cases. Based on the experimental visualization, it can be observed that the development of cloud cavitation has a distinctly quasi-periodic pattern and the periods T_{cycle} of the cloud cavitation is about 40ms, which is corresponding to $5.7c/U_\infty$. Figure 5 presents the measured time evolution of the nomarlized cavity area over several flow cycles at cloud cavitation regimes, which is drawn by an in-house feature-recognition software package [8]. The cavity areas change periodically and the measured mean value are $0.49S_c$, 0.59 S_c and 0.72 S_c respectively, where S_c is the cross-section area of the hydrofoil.

（i）0.125 T_{cycle} （ii）0.25 T_{cycle} （iii）0.375 T_{cycle} （iv）0.5 T_{cycle}

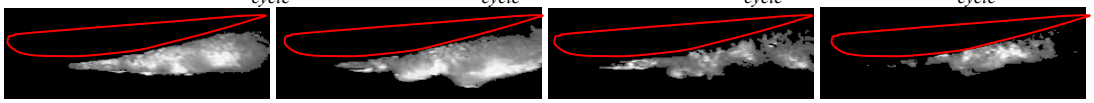

（v）0.625 T_{cycle} （vi）0.750 T_{cycle} （vii）0.875 T_{cycle} （viii）1.0 T_{cycle}

Figure 4 Time evolution of cavity shapes in the typical cloud cavitation regimes (α=8°, σ=0.80).

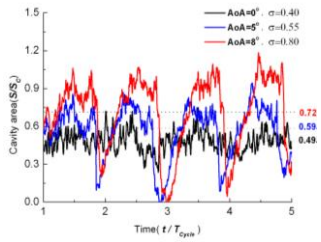

Figure 5 The time evolution of the cavity area.

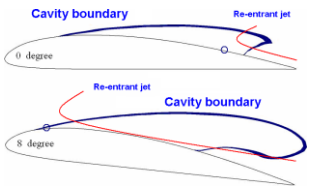

Figure 6 The re-entrant flow in the cavity region

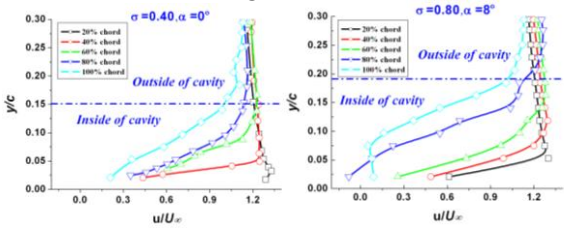

Figure 7 Mean of the ensemble averaged axial velocity profiles at selected chordwise locations.

Figure 6 shows the schematic representation of the re-entrant flow in the region of an attached cavity in typical cloud cavitation regimes. It could be concluded that the cavity thickness is directly controlled by the angle of attack, and the ratio of the thickness of the cavity to that of the re-entrant flow is substantially important to estimate the unsteady behavior of the partial cavity. For σ=0.80 at α=8°, the cavity is thick enough to limit the interaction between the re-entrant flow and the cavity interface, which allows the re-entrant flow to reach the cavity leading edge and the formation of a large scale vapor structures. However, for σ=0.40 at α=0°, because of the smaller cavity thickness, there is a strong interaction between the cavity interface and the re-entrant flow. The re-entrant flow can only reach the rear part of the hydrofoil, contrary to the large scale cloud shed for σ=0.80 at α=8°, the small vapor structures are formed.

3.2. The flow structures in cavitating region

Figure 7 shows the mean values of the normalized ensemble averaged axial (u) velocity profiles at different chordwise locations for σ=0.80 at α=8° and σ=0.40 at α=0°. The Y axis represents the vertical distance from the suction side of the foil. For the case of σ=0.80 at α=8°, recirculation breaks up and lifts the cavity upward, and the large scale shedding is formed, which significantly increases the thickness of the boundary layer and larger low velocity region can be observed compared to the case for σ=0.40 at α=0°. Consequently, the gradients of the mean axial velocity profiles for the σ=0.40 at α=0° case tend to be smaller than that for the σ=0.80 at α=8° case.

With the fluorescent particles in the flow field (seen in figure 8(a), we can capture the turbulent velocity fields, figures 8(b) and (c) show the normalized amplitude of the averaged fluctuating velocities, $I=\sqrt{\overline{u'^2}+\overline{v'^2}}/U_\infty$, where *u'* and *v'* are the horizontal and vertical components of the turbulent velocity fluctuations. For both cases, large velocity fluctuation occurs near the aft half-chord of the hydrofoil and continues into wake, indicating unsteady large-scale fluctuations due to the shedding of the cloud cavity, especially for the σ=0.80 at α=8° case. Meanwhile, the turbulent fluctuations are confined to a thicker layer on the suction side.

(a) the fluorescent particles in the flow field (b) α=0°,σ=0.40 (c) α=8°, σ=0.80

Figure 8 Normalized amplitude of the turbulent velocity fluctuations.

3.3. The hydrodynamics of unsteady cavitating flows

Figure 9 shows the measured lift coefficient (C_L) and drag coefficient (C_D) over a range of non-dimensional parameter σ/2*α*. When the flow is subcavitating, both lift and drag coefficients remain largely unchanged as σ/2*α* varies. In the incipient cavitation stage, the effect of cavitation on the lift and drag coefficients is very small. In the subcavitating and incipient cavitation stages, the hydrodynamic coefficients show little fluctuations due to the relatively stable cavity dynamics, as indicated by the error bars. Further decreasing σ/2*α*, the development of cavitation increases the drag while the lift coefficient becomes lower. In the cloud cavitation stage, the large vortex shedding and related unsteady movement strongly affect the flow structures around the hydrofoil, leading to the relatively higher magnitude of drag and lower magnitude of lift. As indicated by the error bars of the hydrodynamic coefficients in the cloud cavitation stage, the measured values show large fluctuations, especially for the case of α=8°, which is induced by the unstable cavity dynamics. Finally, the flow transitions from cloud cavitation to supercavitation, the cavities exhibits more steady characteristics and both drag and lift coefficients become lower.

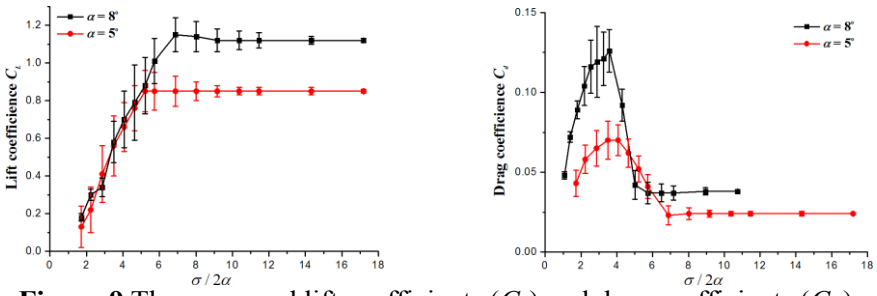

Figure 9 The measured lift coefficients (C_L) and drag coefficients (C_D).

4. Conclusions

The objectives of this paper are to investigate the unsteady structures and hydrodynamic characteristics of the cavitating flows, and to provide experimental data for future numerical validating studies. Experimental studies are presented for a Clark-Y hydrofoil at the fixed angles of attack of α=0°, 5° and 8° with Re=7×10^5 for various cavitation numbers. Detailed analysis of the cavity behavior is applied to identify the re-entrant flow instability which leads to cloud cavitation at different angles of attack. The primary findings include:

(1) Cloud cavity is highly unsteady. For σ=0.40 at α=0°, the thickness of the attached cavity is comparable to the re-entrant flow, a relatively strong interaction exists between the cavity interface and the re-entrant flow throughout its upstream movement. The cavity in the rear part of the hydrofoil splits into small vapor structures. For σ=0.80 at α=8°, the attached cavity is thick enough to limit the interaction between the re-entrant flow and the cavity interface during its movement to the leading edge and the interface is cut, contrary to the small scale cloud shed for σ=0.40 at α=0°, the typical large vapor structures are formed.

(2) Compared to the case for σ=0.40 at α=0°, the velocities in the cavitating region are much lower, and the fluctuating velocities as well as turbulent intensities are much higher for the cloud cavitating case with σ=0.80 at α=8°, which lead to a much thicker turbulent boundary layer.

(3) The dynamic characteristics of the cavitation vary considerably with the angles of attack. The effect of the incipient cavity on the lift and drag coefficients is very small, little fluctuation of the dynamic is obseved. With the decrease of cavitation numbers, the lift and drag coefficients are affected by the cavitating flow structure. At cloud cavitation, the large scale shedding leads to the relatively higher magnitude of drag and decrease of the lift, and the dynamic coefficients exhibit substantial fluctuations. As supercavitation appears, the cavity shapes and dynamics seem more stable.

Acknowledgements

This work was supported by the National Science Foundation of China (Grant No.51306020) and Beijing Natural Science Foundation (Grant No.3144034).

References

[1] Arndt R E A 1981 *Ann. Rev. Fluid Mech.* **13** 273-328.
[2] Ausoni P, Farhat M, Escaler X, Equsquiza E and Avellan F 2007 *ASME J. Fluid Eng* **129** 966-73.
[3] Huang B, Ducoin A and Yong Y L 2013 *Phys. Fluids* **25** 102109.
[4] Wang G, Senocak I, Shyy W, Ikohagi T and Cao S 2001 *Prog. Aero. Sci.* **37** 551-81.
[5] Li X, Wang G, Zhang M and Shyy W 2008 *Int. J. Heat Fluid Flow* **47** 1263-75.
[6] Shridhar G and Katz J 2000 *Phys. Fluids* **12**(4) 895-911.
[7] Huang B 2012 *Thesis of PhD* Beijing Institute of Technology.
[8] Zhang M, Song X and Wang G 2006 *Trans. Beijing Inst. Technol.* **26** 983-6.